Land Surface Model Development for the GISS GCM: Effects of Improved Canopy Physiology on Simulated Climate

ANDREW D. FRIEND

Laboratoire des Sciences du Climat et de l'Environnement, Gif-sur-Yvette, France

NANCY Y. KIANG

Center for Climate Systems Research, Earth Institute, Columbia University, NASA Goddard Institute for Space Studies, New York, New York

(Manuscript received 18 August 2004, in final form 30 December 2004)

ABSTRACT

A new physiology-based model of canopy stomatal conductance and photosynthesis is described and included in the latest version of the Goddard Institute for Space Studies (GISS) GCM, ModelE1. The submodel includes responses to atmospheric humidity and CO_2 concentration, responses missing from previous GISS GCM land surface schemes. Measurements of moisture, energy, and CO_2 fluxes over four vegetation types are used to test and calibrate the submodel. Photosynthetic leaf N is calibrated for each vegetation type from the flux measurements.

The new submodel results in surface cooling over many regions previously too warm. Some warm biases of over 2°C are cooled by more than 0.5°C, including over central Eurasia, South America, the western United States, and Australia. In addition, some regions that were previously too cool are warmed, such as northern Eurasia and the Tibetan Plateau. A number of precipitation biases are also reduced, particularly over South America (by up to 1 mm day^{-1}) and the oceanic ITCZs (by over ± 1 mm day^{-1}); coastal west Africa becomes significantly wetter. Cloud cover increases over many land areas previously too clear.

Higher absolute canopy conductances, and positive feedbacks with atmospheric humidity, are largely responsible for the simulated vegetation influence on the atmosphere. High-latitude climate changes through remote effects of increased tropical latent heating, resulting directly from improved characterization of tropical forest canopy conductance. Realistic representation of the stomatal control on land evaporation is critical for accurate simulation of atmospheric dynamics in the GISS GCM.

1. Introduction

Vegetation processes determine the partitioning of energy and moisture over much of the global land surface and therefore require realistic representation in models designed to simulate climate dynamics over decadal to century time scales (Hollinger et al. 1994). The complexity of vegetation representations in GCMs has greatly increased over the last decade (e.g., Bonan 1995; Foley et al. 1996; Sellers et al. 1996; Cox et al. 1999; Dickinson et al. 2002). The National Aeronautics and Space Administration (NASA) Goddard Institute for Space Studies (GISS) GCM contains state-of-the-art representations of many components of the climate system but has lacked a sophisticated representation of vegetation. This paper describes the first stage in addressing this deficiency through the introduction of a physiology-based canopy stomatal conductance and photosynthesis scheme, and examines consequences for simulated climate.

The loss of water from most terrestrial plant leaves is strongly limited by the presence of a highly impermeable waxy cuticle. To allow fixation of CO_2, stomatal pores open under conditions favorable for photosynthesis, causing an unavoidable loss of water from the inner tissue. This conflict between the requirement for CO_2 fixation, and the negative effect of desiccation on physiological processes, has resulted in strong biological control of evaporation over vegetated surfaces (Hetherington and Woodward 2003).

Stomatal pores change aperture in response to a wide

Corresponding author address: Dr. Andrew D. Friend, Laboratoire des Sciences du Climat et de l'Environnement—Orme, Bât. 712, Orme des Merisiers, F-91191 Gif-sur-Yvette Cedex, France. E-mail: friend@lsce.saclay.cea.fr

range of environmental stimuli, including light, temperature, soil moisture, atmospheric humidity, and atmospheric CO_2 (Zeiger et al. 1987). However, the mechanisms whereby stomata respond to these signals are complex and not well understood. In addition, nonlinear physiological responses and small-scale physiological and environmental variability greatly complicate the scaling of leaf processes to the canopy, landscape, and region or GCM grid box.

Models of stomatal behavior range from purely empirical (e.g., Jarvis 1976), to mixed empirical/mechanistic (e.g., Ball et al. 1987), to optimality models (e.g., Cowan and Farquhar 1977; Friend 1995). Recently, detailed mechanistic models of stomatal behavior have been developed, such as that of Buckley et al. (2003); these hold much promise but are as yet too complex for GCMs.

Eddy flux data are now available for many vegetation types. These data typically comprise surface fluxes (e.g., latent and sensible heat and CO_2), their meteorological drivers (radiation, temperature, and atmospheric turbulence and humidity), plant physiological status (e.g., leaf N content) and its spatial variation, and vegetation structure (e.g., leaf area and canopy height; Baldocchi et al. 2001), and present a unique opportunity to test and parameterize canopy-scale models of surface fluxes for use in GCMs.

Here we describe a new model of vegetation canopy stomatal conductance designed for use in GCMs. The model is tested and calibrated using eddy flux data. It seeks to improve on earlier canopy conductance models by focusing on direct driving variables and the spatial interactions between photosynthetic N and light.

In the following sections we describe the previous GISS GCM canopy stomatal conductance submodel and the derivation of the new approach. We then test both submodels using flux measurements made over four different vegetation types and calibrate one of the new submodel's parameters to account for vegetation-specific physiology. We then extend this calibration to all vegetation types in the GCM, and perform a global climate integration with the latest frozen version of the GISS GCM, comparing predicted climate with an integration using the old conductance scheme. Mechanisms for the effects of the new submodel on climate are discussed.

2. Methods

a. Former GISS GCM approach to canopy stomatal conductance

Abramopoulos et al. (1988) described a relatively complex ground hydrology scheme for the GISS GCM, with explicit treatment of transpiration, to which was later added an empirical representation of canopy stomatal conductance (Rosenzweig and Abramopoulos 1997),

$$g_{\text{can\_RA}} = \beta_D \frac{L_{\text{eff}}}{r_{s,\min}} \frac{\left(\frac{R_g}{R_g + 90}\right)}{1 + \left(\frac{T_c - 23}{15}\right)^4}, \qquad (1)$$

where $g_{\text{can\_RA}}$ is canopy stomatal conductance (m s^{-1}), β_D is a soil moisture availability factor (fraction), L_{eff} is effective leaf area index (LAI; scaled from projected LAI to account for canopy light distribution; Abramopoulos et al. 1988) [$m^2_{(\text{leaf})}$ $m^{-2}_{(\text{ground})}$], $r_{s,\min}$ is a vegetation-specific minimum leaf stomatal resistance (s m^{-1}), R_g is incident shortwave radiation (W m^2), and T_c is canopy temperature (°C). Factor β_D is a linear function of the rooting density–weighted water potential in each soil layer. Submodel (1) is referred to as "RA97" in the rest of this text, and its response to various forcings is shown in Fig. 1.

GISS GCM vegetation categories and global distributions are described by Matthews (1983, 1984), and comprise tundra, grassland, shrub (i.e., dry savanna), woodland (i.e., medium and wet savanna), deciduous (forest/woodland), evergreen (non–rain forest), rain forest (tropical), and crops. Each category is assigned values for annual maximum and minimum LAI, $r_{s,\min}$, and total canopy height (Table 1). In addition, vegetation-specific parameters specify rooting distributions (Rosenzweig and Abramopoulos 1997) and seasonal albedos (Hansen et al. 1983). Each parameter is composited across vegetation types in each land surface gridbox. The LAI of the vegetated fraction in each gridbox varies sinusoidally between the composited annual maximum and minimum values.

b. New approach to canopy stomatal conductance

RA97 omits responses to atmospheric humidity and CO_2, responses likely to be of major importance for land surface–atmosphere interactions in future climates (e.g., Jacobs 1994; Friend and Cox 1995). It also lacks mechanistic responses to light, leaf N, and temperature. Here, a new approach uses understanding gained from leaf and canopy flux measurements, and from physiological studies of photosynthesis, a process closely linked to stomatal conductance. The relative responses of stomatal conductance to soil moisture, atmospheric humidity, CO_2, and canopy height (through its effect on leaf hydrology) are assumed equal for all leaves and are therefore applied directly at the canopy level. However, the complex nonlinear interactions between the responses to light, temperature, and photosynthetic N ne-

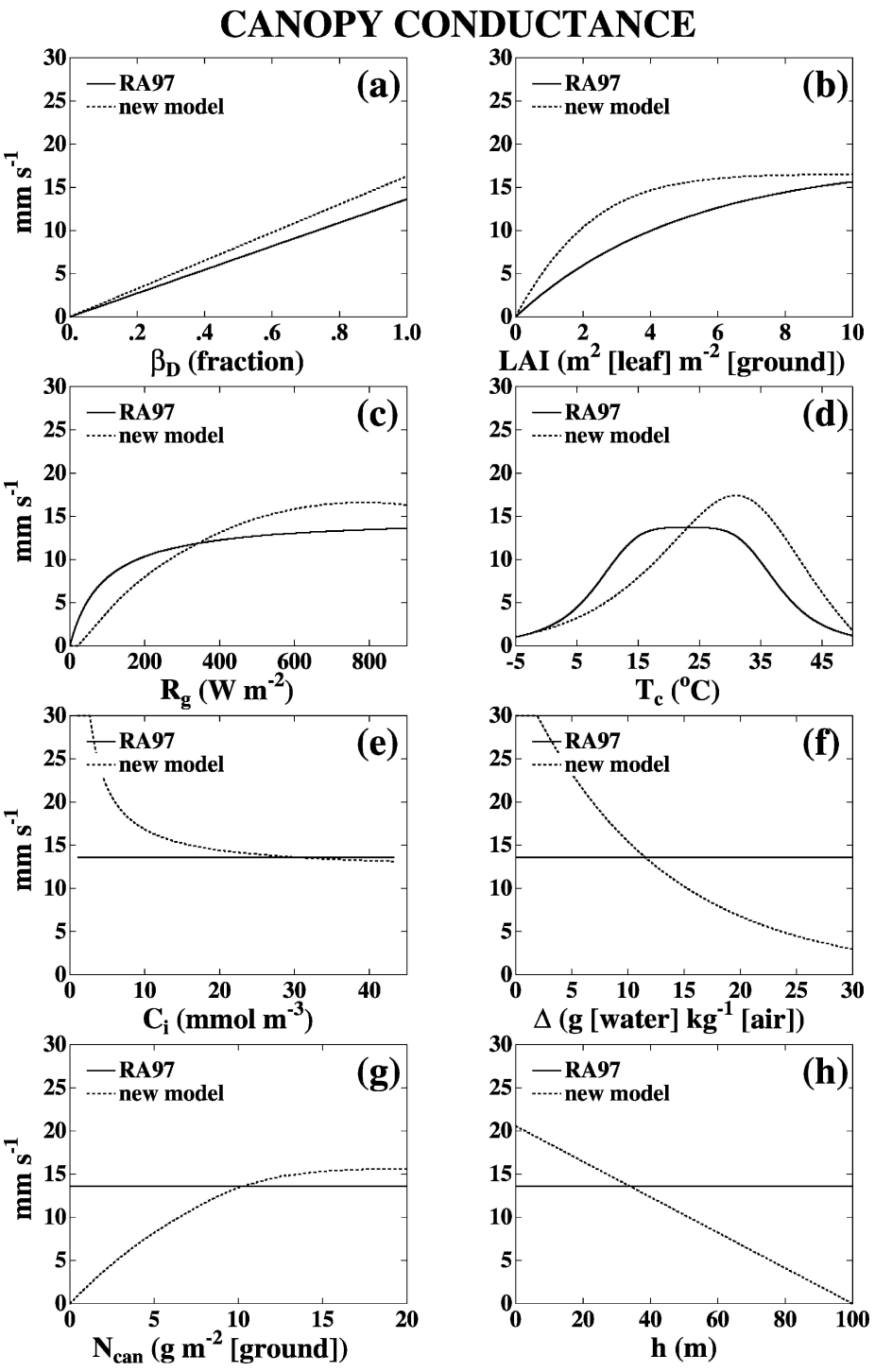

FIG. 1. RA97 (solid line) and new (dotted line) canopy stomatal conductance submodel responses to (a) soil moisture availability, (b) LAI (with varying canopy N), (c) incident downward shortwave radiation, (d) canopy temperature, (e) internal leaf CO_2 concentration, (f) specific humidity gradient across the leaf surface, (g) total canopy N, and (h) canopy height. The latter four factors were not included in RA97. Nonabscissa vegetation-specific variables held at rain forest values: $r_{s,\min} = 250$ s m^{-1}, LAI = 7 $m^2_{(leaf)}$ $m^{-2}_{(ground)}$, $n_f = 1.1$, mean leaf N = 2.3 g m^{-2}, and canopy height = 25 m. Nonabscissa environmental variables held at typical rain forest values: $\beta_D = 1$, $R_g = 900$ W m^{-2}, $T_c = 27$°C, $\Delta = 10$ $g_{(water)}$ $kg^{-1}_{(air)}$, $C_i = 0.0113$ mol m^{-3}, atmospheric pressure = 101 325 Pa, lat = 3°N, yearday = 180, and solar time = 1200.

TABLE 1. Vegetation parameters in original and new GISS GCM land surface schemes. LAI_{max} and LAI_{min} are annual max and min LAIs, $r_{s,min}$ is min leaf resistance to moisture flux, and height refers to total canopy height. Mean leaf N derived from White et al. (2000), except for rain forest, taken from Carswell et al. (2000), and crops, taken from measurements on wheat (J. Berry 2004, personal communication). White et al. (2000) reported mean values for specific leaf area (SLA; i.e., leaf area per unit C) and leaf C:N ratio for North American species, from which N content was calculated for deciduous broadleaf forest (deciduous), evergreen needleleaf forest (evergreen), shrub, and grass (grassland); Berry's SLA and C:N data were used for crops. Calibration against flux data (see text and Table 2) gave values for the photosynthetic N factor (n_f) for deciduous (Harvard Forest), evergreen (Bray), rain forest (Manaus), and crops (Ponca) vegetation types. Values for other types were estimated: grassland = deciduous (both are dominated by angiosperms with short-lived broad leaves); woodland is largely savanna = (grassland + rain forest)/2; shrub = woodland; and tundra = (grassland + shrub)/2.

	Tundra	Grassland	Shrub	Woodland	Deciduous	Evergreen	Rain forest	Crops
Original GCM parameters								
LAI_{max}	1.5	2	2.5	4	6	10	8	4.5
LAI_{min}	1	1	1	1	1	8	6	1
$r_{s,min}$ [s $m^{-1}_{(H2O)}$]	100	100	200	200	200	300	250	125
Height (m)	0.1	1.5	5	15	20	30	25	1.75
New canopy stomatal conductance submodel parameters								
Mean leaf N (g m^{-2})	1.6	0.82	2.38	1.03	1.25	2.9	2.7	2.5
n_f	1.4	1.5	1.3	1.3	1.5	0.9	1.1	1.3

cessitates integration over leaf classes, with varying light and physiological characteristics (Friend 2001). The following sections detail how these responses are represented in the new submodel.

1) CONDUCTANCE RESPONSES TO LIGHT, TEMPERATURE, AND N

(i) General background

The ratio of CO_2 concentration between internal leaf air spaces (C_i) and the air outside the leaf (C_a) remains fairly constant as light and temperature vary (Wong et al. 1979), indicating that the response of stomata to these variables is proportional to the response of net photosynthesis. This proportionality is the basis of many models of stomatal conductance, in which stomatal aperture is related directly to net photosynthesis (e.g., Ball et al. 1987; Jacobs et al. 1996). However, this assumed relationship, and the value given to the ratio, have a dominating effect on predictions (Friend et al. 1993), and observations frequently show departures from this constancy (e.g., Carswell et al. 2000). Therefore, the new submodel allows this ratio to vary by modeling stomatal conductance and photosynthesis separately, but linked to maintain C_i at a value commensurate with the physiological capacity for its fixation.

This linkage is represented by equating the relative stomatal responses to light, temperature, and photosynthetic N to those of the responses of photosynthetic capacity to these forcings. Photosynthetic capacity is defined as the rate at which net photosynthesis could proceed if it were not limited by CO_2. This assumption is consistent with the experimental analysis of Wong et al. (1979), who concluded that C_i alone is unable to mediate information on photosynthetic capacity.

Jarvis and Davies (1998) and Buckley et al. (2003) used these arguments to derive models of stomatal conductance that include dependencies on the rate of net photosynthesis at saturating C_i, similar to the model proposed here. Their models assume that stomata respond to the excess in photosynthetic capacity, rather than an absolute value. However, these two models, and the one proposed here, have the common feature that, to quote Buckley et al. (2003), "stomata respond positively to some measure of how much faster CO_2 could be fixed if stomata did not limit its supply."

To ensure both realism in the behavior of canopy conductance and the ability to parameterize from physiological information, a physiology-based model of canopy radiation and photosynthesis is used to calculate the distribution of photosynthetic capacity over the canopy.

(ii) Canopy radiation

The vertical distribution of canopy radiation in the new model follows the approach of Spitters et al. (1986), as implemented by Friend (2001), wherein radiation absorbed by sunlit and shaded foliage, and their relative areas at each canopy level, are calculated from LAI, solar elevation, and downwelling direct and diffuse radiation above the canopy. Total photosynthetically active radiation [PAR; $\mu mol_{(quanta)}\ m^{-2}_{(ground)}\ s^{-1}$] is taken as $2.3 \times R_g$, with R_g (W m^{-2}) and the fractions of direct and diffuse incident PAR taken from the GCM. Canopy extinction coefficients for diffuse and

direct PAR are calculated using the method of Spitters (1986), assuming a spherical leaf angle distribution and random leaf position. Canopy reflection assumes a green closed canopy (Spitters et al. 1986).

(iii) Photosynthesis and respiration

Gross (i.e., CO_2 fixation minus photorespiration, but not including mitochondrial respiration) photosynthetic capacity for each leaf class is calculated using the model of Kull and Kruijt (1998), applied at the limit C_i = infinity. This model is based on that of Farquhar et al. (1980) and von Caemmerer and Farquhar (1981), but treats light extinction through individual leaves to separate light-saturated and light-limited chloroplasts, with light absorption and photosynthesis expressed on an N basis for scaling to the leaf. Therefore, this model not only realistically describes leaf-level responses to light, but it also enables scaling to the canopy using the vertical distribution of leaf N (Friend 2001) and application to different vegetation types using their different photosynthetic N contents (see below). In addition, this approach avoids the need for an empirical smoothing function between the Rubisco- and RuBP-limited rates of photosynthesis, a nonmechanistic approach that has a significant influence on predicted photosynthesis (Friend 1995).

Parameter values for the photosynthesis model are taken from Kull and Kruijt (1998) and Bernacchi et al. (2001), except for vegetation-specific values for leaf N and ratios of electron transport capacity and Rubisco catalytic capacity to leaf N. Absolute values and temperature functions for Rubisco kinetic parameters are taken from Bernacchi et al. (2001), and the temperature dependency of electron transport is taken from Friend (1995).

The canopy N profile follows a negative exponential decline with depth, with an extinction coefficient (0.11) fitted to the tropical rain forest observations of Carswell et al. (2000) and applied to all vegetation types. The profile of the chlorophyll/N ratio is fitted to data presented by Kull and Kruijt (1998):

$$n_3 = 6 - 3.6e^{-0.7L_c}, \tag{2}$$

where n_3 has units of $\mu mol_{(Chl)}\ g_{(N)}^{-1}$, and L_c is cumulative LAI from the top of the canopy.

Gross photosynthetic capacity at each canopy level is weighted across sunlit and shaded fractions. Integration across canopy levels uses Simpson's rule (Press et al. 1989), with a tolerance on the canopy CO_2 flux error of 0.1 $\mu mol_{(CO2)}\ m^{-2}\ s^{-1}$.

Leaf mitochondrial respiration is assumed to vary linearly with N, with proportionality calculated from the rain forest measurements of Carswell et al. (2000) to be 0.2 $\mu mol_{(CO2)}\ s^{-1}\ g_{(N)}^{-1}$. The temperature response of Bernacchi et al. (2001) is used. Canopy net photosynthetic capacity (A_{cap}) is then the difference between canopy gross photosynthetic capacity and canopy respiration (R_{can}), and quantifies canopy stomatal conductance responses to light, temperature, and photosynthetic N.

2) CONDUCTANCE RESPONSE TO ATMOSPHERIC HUMIDITY

Stomatal conductance declines with an increasing gradient of atmospheric specific humidity between the internal leaf air spaces and the air on the outer leaf surface (Δ) (e.g., Mott and Parkhurst 1991; Jones, 1992). The response is equivalent to a linear increase in stomatal resistance with Δ. Net photosynthesis has a saturating response to C_i, and therefore a linear decline in C_i/C_a with Δ is generally observed and is used as the basis for many stomatal conductance models (e.g., Jacobs et al. 1996). However, the slope and intercept of this relationship are not fixed, implying that C_i/C_a varies with forcings other than only Δ. Therefore, the conductance response to Δ is included here explicitly but is parameterized to produce an approximately linear decline in C_i/C_a over the normal range of field Δ values, giving

$$f_\Delta = 2.8^{-80\Delta}, \tag{3}$$

where f_Δ is relative canopy conductance, and Δ has units of $kg_{(water)}\ kg_{(air)}^{-1}$. It is assumed that all canopy leaves react identically to changes in Δ, and therefore f_Δ is applied directly at the canopy level.

3) CONDUCTANCE RESPONSE TO CO_2

Stomata are frequently observed to close in response to increasing atmospheric CO_2 (e.g., Morison 1998). The signal seems likely to be a metabolic product that is reduced as C_i increases (e.g., Buckley et al. 2003). Forstreuter (1998) measured the relationship between leaf stomatal conductance and C_i in European beech (*Fagus sylvatica* L.), and the following fit to his results is used here:

$$f_{CO_2} = \frac{C_i + 0.004}{5C_i}, \tag{4}$$

where f_{CO2} is relative canopy conductance, scaled to unity at C_i = 0.001 $mol_{(CO2)}\ m^{-3}$. Concentration C_i is assumed constant with canopy depth, and therefore f_{CO2} is applied directly at the canopy level.

4) CONDUCTANCE RESPONSE TO CANOPY HEIGHT

Stomatal opening requires positive turgor, and a hydrostatic gradient exists up tree stems, which increases

during transpiration. It is therefore believed that tree height is ultimately limited by water transport (Friend 1993; Koch et al. 2004). If the mean canopy leaf is held at 75% of total height, then as the tallest observed trees are about 100 m:

$$f_h = 1 - 0.0075h, \tag{5}$$

where f_h is the relative effect of canopy height on canopy stomatal conductance, and h is total plant height (m).

5) Complete canopy stomatal conductance model

The various component responses detailed above are combined multiplicatively to give overall canopy stomatal conductance to moisture, using bulk canopy values for Δ and C_i and linear scaling with A_{cap}:

$$g_{\text{can}} = \alpha\beta_D f_\Delta f_{\text{CO}_2} f_h A_{\text{cap}}, \tag{6}$$

where g_{can} is total canopy stomatal conductance to moisture, and α is a constant of proportionality [$\text{m}^3_{(\text{H2O})}\ \text{mol}^{-1}_{(\text{CO2})}$; calibrated from observations; see below]. The effect of soil moisture is included as in RA97.

6) Solving for C_i, Δ, and limits to conductance

The concentration C_i [(4)] is carried across time steps by balancing bulk canopy net CO_2 supply and fixation

$$A_{\text{can}}(t-1) = \frac{C_s(t-1) - C_i(t)}{r_{\text{tot}}(t-1)}, \tag{7}$$

where A_{can} is canopy net photosynthesis, C_s is atmospheric CO_2 at the surface level of the GCM, and r_{tot} is the combined bulk canopy stomatal and atmospheric resistance to CO_2 flux from the surface level to the internal leaf air spaces. The maximum land surface model time step is 30 min, and the relatively long time constant for stomatal movements (see below) therefore justifies this carryover. If a solution for C_i is negative, C_i is set to half its previous value; in addition, C_i is limited to values $\geq$0.1 mmol m^{-3}. These two measures ensure stability and physical realism.

Flux A_{can} is calculated as for A_{cap} but evaluated at $C_i(t-1)$; r_{tot} is taken as

$$r_{\text{tot}} = \frac{1.42}{g_{\text{can}}} + \frac{1.65}{C_h U}, \tag{8}$$

where C_h is the atmosphere transfer coefficient between the canopy and the atmosphere surface level (unitless), and U is horizontal wind speed (m s^{-1}). The constants convert resistance units from water to CO_2 (Monteith 1973).

The gradient Δ is also carried across time steps, implicitly allowing stomata time to adjust to a change in leaf water status (and ensuring stability):

$$\Delta(t) = q_{\text{can}}(t) - q_f(t-1), \tag{9}$$

where q_{can} is internal leaf air space–specific humidity (assumed saturated), and q_f is bulk canopy leaf surface specific humidity, calculated by balancing the moisture flux to the surface level:

$$E = \rho C_h U(q_f - q_s), \tag{10}$$

where E is canopy transpiration, ρ is atmospheric density, and q_s is GCM surface level specific humidity. Humidity, q_s is solved by the GCM on each time step (Rosenzweig and Abramopoulos 1997), and Δ is limited to positive solutions.

Canopy stomatal conductance is limited to the range 0.06 $\times$ to 6 $\times$ LAI $\text{mm}_{(\text{H2O})}\ \text{s}^{-1}$, based on observed values (Nobel 1991). It is further assumed that it takes a minimum of 30 min for the stomata to change aperture between these two limits (Mencuccini et al. 2000), limiting $|\partial g_{\text{can}}/\partial t|$ to $\leq$0.0033 $\times$ LAI $\text{mm}_{(\text{H2O})}\ \text{s}^{-2}$.

c. Comparison of old and new canopy stomatal conductance submodels

The response of the new canopy stomatal conductance scheme to environmental forcings is also shown in Fig. 1. Biological and physical forcings are specified for tropical rain forest conditions for both models. The new model predicts 20% higher conductance under standard conditions (Fig. 1a) and a much more rapid initial increase with LAI (Fig. 1b). Little increase occurs above an LAI = 4, whereas RA97 is more linear. All available PAR is absorbed at an LAI $\approx$ 6 in the new model.

The new model predicts a more gradual increase in conductance with incident light (Fig. 1c). This is due to the more realistic canopy radiation and photosynthesis schemes, wherein increasing incident light increases light penetration at both canopy and leaf levels. A slight fall in total conductance occurs at high light because of a lower diffuse fraction.

The temperature response of RA97 has a very broad optimum (Fig. 1d), whereas the biochemical temperature responses in the new model result in a rather narrow optimum around 31°C. This parabolic shape is typical of measured leaf-level physiological responses, with steep declines in CO_2 uptake above 31°C even in tropical tree species (Clark 2004).

The last four forcings shown in Fig. 1 are not present in RA97: internal leaf CO_2 (Fig. 1e), humidity gradient across the leaf surface (Fig. 1f), total canopy N (Fig. 1g), and canopy height (Fig. 1h). Conductance declines

TABLE 2. Flux datasets and associated parameters used to test canopy stomatal conductance and photosynthesis model. LAI is projected. LAI and canopy N for Bray are tree + grass. See main text for derivation of other parameters.

Site	Manaus	Bray	Harvard Forest	Ponca
Full name	Reserva Biológica do Cuieiras	Le Bray	Harvard Forest	Ponca
Location	Amazonas, Brazil	Near Bordeaux, France	Petersham, MA	Ponca City, OK
Coordinates	2°35′ S, 60°07′ W	44°42′ N, 0°46′ W	42°32′N, 72°10′W	36°46′ N, 97°8′ W
Primary reference	Malhi et al. (1998)	Berbigier et al. (2001)	Wofsy et al. (1993)	Hanan et al. (2002)
Flux data source	Yadvinder Malhi, University of Edinburgh, United Kingdom	Paul Berbigier, INRA Bioclimatologie, Bordeaux, France	Goulden et al. (1996), Ameriflux Web site[g]	Ameriflux Web site[g]
Period	13–20 Nov 1995	11–20 May 1998	14–23 Aug 1996	3 Mar–11 Jun 1999
Canopy CO_2 storage measured?	Yes	No	Yes	No
Dominant species	Mixed rain forest[b]	*Pinus pinaster* Ait., *Molinia coerula* L. Moench	Mixed oak/maple	*Triticum aestivum* L.
Age (yr)	Mixed[b]	28[c]	60–70[g]	0.02–0.27[k]
LAI [$m^2_{(leaf)}$ $m^{-2}_{(ground)}$]	6.1[a]	1.37[d] + 1.45[e]	3.5[h]	0.1–4.7 [k]
Canopy N [g $m^{-2}_{(ground)}$]	16[a]	6.4[d] + 0.8[c, e]	6.7[h, i]	0.03–11.6[k]
Canopy height (m)	30[a]	18[d]	24[g]	0.13–0.96 [k]
Measurement height (m)	46.5[b]	25.5[f]	30[g]	4.5[g]
Roughness length (m)	2.0[a]	1.8[f]	1.5	0.02–0.13
Time step (h)	1	0.5	1	0.5
Soil moisture (β_D: fraction)	0.86	1.0	0.95	1.0[k]
Mean soil temperature (°C)	24.5	16.0	17.0	13.7
Soil temperature depth (cm)	5	5	"Near surface"	10
Noncanopy respiration at 25°C [RE: $\mu mol_{(CO2)}$ m^{-2} s^{-1}]	3.44	8.8	6.3	9.1
Relative photosynthetic N (n_f)	1.1	0.9	1.5	1.3

[a] Data from Williams et al. (1998).
[b] Data from Malhi et al. (1998).
[c] Data from Berbigier et al. (2001).
[d] Data from Porté and Loustau (1998), assuming reported LAI is all sided.
[e] Data from Loustau and Cochard (1991).
[f] Data from the Fluxnet Web site (http://www.fluxnet.ornl.gov/fluxnet/webpage2url.cfm?KEYID=fr.Bordeaux.01).
[g] Data from Ameriflux Web site (http://cdiac.esd.ornl.gov/ftp/ameriflux/).
[h] Data from Amthor et al. (1994).
[i] Data from Aber et al. (1993).
[j] Data from G. Burba (2004, personal communication).
[k] Data from J. Berry (2004, personal communication).

steeply with Δ, typical of responses measured in the field (Jones 1992).

d. Model testing and parameterization of vegetation types

The complete canopy stomatal conductance and photosynthesis model was tested using fluxes measured over four of the major vegetation types specified in the GCM: tropical rain forest (near Manaus, Brazil), evergreen needleleaf forest (Le Bray, near Bordeaux, France), cold deciduous forest (Harvard Forest, Massachusetts), and cropland (Ponca, Oklahoma). Details of each site and the periods selected are given in Table 2.

Values of bulk canopy temperature, stomatal conductance, net photosynthesis, and leaf surface humidity and CO_2 concentrations for testing and calibrating the model were calculated using aerodynamic expressions for the vertical movement of heat, moisture, and CO_2, assuming equality between their aerodynamic transfer coefficients and including estimates of noncanopy components (see following sections).

1) INVERTING FLUX MEASUREMENTS TO INFER CANOPY PROPERTIES

(i) Canopy temperature and stomatal conductance

Canopy temperature and the atmospheric transfer coefficient (C_h) were solved from the measured sen-

sible heat flux using the drag law parameterization and the Monin–Obukhov similarity relations for the dependence of the heat flux on the bulk Richardson number (Deardoff 1967; Hansen et al. 1983). Unrealistic solutions were discarded.

Roughness length and measurement height were maintained at site-specific values (Table 2). At Manaus, the level of zero plane displacement was solved at each time step using an expression for the wind profile (Oke 1987). Friction velocity was not directly reported for Bray or Harvard Forest and was therefore calculated from the measured momentum flux (Oke 1987). This procedure greatly increased the number of valid solutions (probably because of the dependence of zero plane displacement on wind speed). For Ponca, the zero plane displacement and roughness length were calculated using the relationships of Choudhury et al. (1986).

Bulk canopy stomatal conductance to moisture was then estimated from the measured moisture flux, assuming that stomatal and atmospheric transfer occur in series and all water originates from within leaves (favored by selecting observational periods with no or low rainfall):

$$E = \frac{\rho(q_{\text{can}} - q_s)}{\dfrac{1}{g_{\text{can}}} + \dfrac{1}{C_h U}}. \tag{11}$$

(ii) Canopy CO_2 flux

Net canopy CO_2 flux (A_{can}) and canopy leaf surface CO_2 concentration (C_f) were estimated from the measured vertical CO_2 flux (F_c), canopy air space storage of CO_2 (F_{store}), where measured (Table 2), and estimated noncanopy respiration (RE):

$$A_{\text{can}} = \text{RE} - (F_c + F_{\text{store}}) = C_h U(C_s - C_f). \tag{12}$$

Respiration at 25°C was calibrated at each site to measured CO_2 fluxes during turbulent nights (Table 2) and forced by measured soil temperature using the temperature response measured by Meir et al. (1996).

(iii) Inverted canopy stomatal conductance and CO_2 flux

Inferred mean diurnal cycles of bulk canopy stomatal conductance and transpiration (assumed equal to the measured moisture flux) are shown for each site in Fig. 2. Transpiration is remarkably similar between sites, whereas peak conductance varies considerably, reflecting differences in atmospheric humidity. The asymmetric conductance responses, with lower afternoon values despite similar moisture fluxes, also reflect variations in Δ. Relatively high nighttime canopy conductances reflect moisture flux in a stable atmosphere and are most likely artifacts due to moisture sources other than internal leaf air spaces (e.g., soil and advection).

Inferred A_{can} and modeled RE are also shown in Fig. 2. The poor fits of RE to nighttime A_{can} for Bray and Ponca probably reflect the lack of storage measurements at those sites.

2) Testing and calibrating the canopy model

(i) Canopy model parameterization and forcing at flux tower sites

An offline version of the canopy model was parameterized for each site using observed LAI, canopy N, canopy height, and latitude (Table 2). Forcing was provided by observed R_g, atmospheric pressure, times of year and day, and inverted estimates of bulk canopy temperature, Δ, and C_f. Diffuse fraction was estimated from the ratio of observed R_g to its theoretical maximum given solar elevation and latitude (Spitters et al. 1986). The offline model calculates C_i across time steps [(7)].

It was necessary to estimate the soil moisture availability factor (β_D) from locally available field data. At Manaus, measured volumetric water content was 0.42 $m^3\ m^{-3}$ during the simulation period (Malhi et al. 1998, their Fig. 9), equivalent to $\beta_D = 0.86$ for a clay soil (Abramopoulos et al. 1988). At Bray, the water table in winter is close to the surface, and the measurement period was early in the year following substantial periods of precipitation; β_D was therefore set to 1. At Harvard Forest, mean β_D was calculated from volumetric water contents across six local sites (Davidson et al. 1998) to be 0.925 during May 1996, assuming a loamy soil and accounting for the substantial rain between May and the measurement period. At Ponca, β_D was calculated from observed soil moisture content (G. Burba 2004, personal communication) to equal 1.

The canopy conductance model parameter α [(6)] was defined during the calibration procedure (see following section).

(ii) Canopy flux tower site model simulations and calibration

Manaus site simulations match well the time series of inverted bulk canopy stomatal conductance, transpiration, and CO_2 flux with α set to 3.25×10^3 $m^3_{(H2O)}$ $mol^{-1}_{(CO2)}$. Changing α from this value causes divergent errors in modeled photosynthesis and conductance. Figure 2 shows the binned diurnal cycle, to which the fit is poorer for transpiration than conductance because of small overestimations of conductance at high Δ.

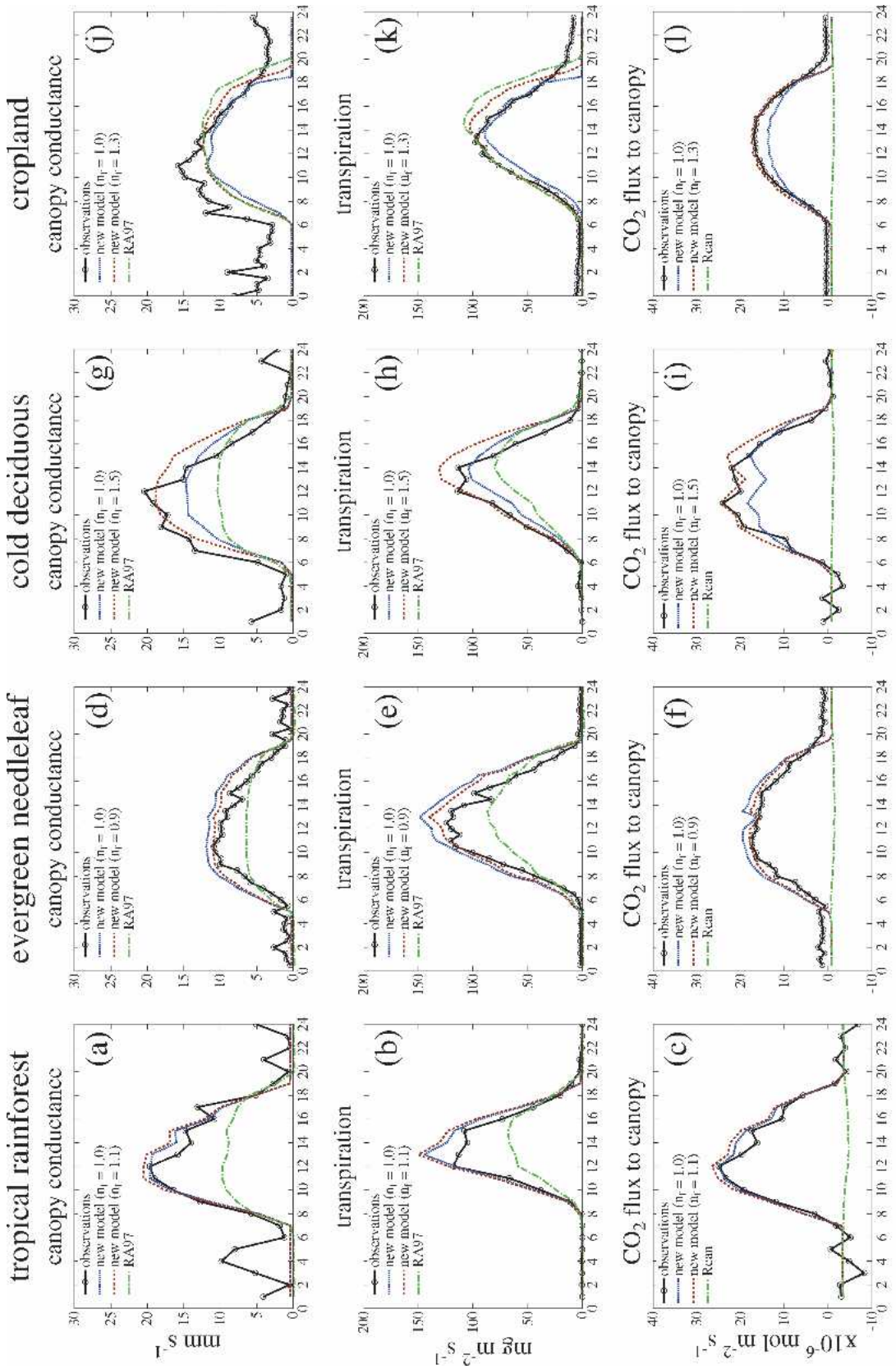

FIG. 2. Binned mean inverted diurnal cycles of canopy stomatal conductance to moisture, transpiration, and canopy net CO_2 flux at each measurement site (Table 2; tropical rain forest refers to Manaus, evergreen needleleaf refers to Bray, cold deciduous refers to Harvard Forest, and cropland refers to Ponca). Values not included in binning of any variable where one was an obvious outlier. Also shown are predictions using model RA97, the new canopy stomatal conductance/photosynthesis model with $n_f = 1$ and with calibrated n_f, and modeled canopy respiration (R_{can}). Calibration of n_f performed to peak canopy net CO_2 flux.

The model was then found to perform reasonably well at Bray (Figs. 2d,f), but to substantially underpredict conductance and photosynthesis at Harvard Forest (Figs. 2g,i). The fraction of leaf N allocated to photosynthetic compounds is an important source of physiological variation between plant types (Friend et al. 1997). Therefore, a coefficient (n_f) to account for this variation was added to the model and applied to the values for the ratios of electron transport capacity and Rubisco catalytic capacity to leaf N.

The coefficient n_f was calibrated independently for each of the four sites against peak mean diurnal A_{can}. The resulting values for n_f are given in Table 2, and new binned diurnal predictions are shown in Fig. 2. After this calibration, the fits are reasonable at each site for both conductance and photosynthesis, although a tendency to overestimate afternoon transpiration remains, possibly related to increasing in situ hydrological stress during the day (Williams et al. 1998).

RA97 bulk canopy stomatal conductances are much lower than in situ values at each site except Ponca (Fig. 2). At Manaus, for example, peak in situ and new model conductances are about 50% greater than RA97 predictions. About 60% of this difference can be accounted for by the humidity response, and the rest by the radiation/LAI response (cf. Fig. 1). RA97 can be forced to match inferred peak conductances by reducing $r_{s,\min}$ [(1)], but afternoon transpiration is then substantially overestimated because of high humidity deficits.

3) Implementation of the new conductance scheme in the GCM

For implementation of the new canopy stomatal conductance scheme in the GCM, n_f was assigned the values derived above for deciduous forest (Harvard Forest), evergreen needleleaf (Bray), rain forest (Manaus), and crops (Ponca). Parameter values and mean leaf N contents for the other four vegetation types were calculated from these values and other published data (Table 1).

e. Climate integrations

Climate integrations were performed with the GISS GCM ModelE1, a complete rewrite of previous GISS models incorporating numerous improvements in basic physics, the stratospheric circulation, and forcing fields (Schmidt et al. 2004, manuscript submitted to *J. Climate*, hereafter SCH). A description of the model physics in the previous version of the GISS GCM is given by Hansen et al. (2002) and the references therein. A 65-m slab ocean was used (Hansen et al. 1983), and initial conditions were specified as the final state of a previous 20-yr integration using an atmospheric concentration CO_2 of 290.7 ppmv (1880 value). Ocean heat fluxes were derived from an average of years 6–15 of this spinup.

Two 30-yr model integrations were performed at CO_2 = 290.7 ppmv: a control using RA97 (O1), and an integration using the new canopy stomatal conductance submodel (N1). The GCM was in energy balance after 10 yr, and subsequent annual means of regional surface energy fluxes showed no trend. Predicted climatologies were taken as the mean of the second decade.

3. Climate data

High-quality globally gridded data exist only for the contemporary period. The likely bias due to comparing modeled and actual climate systems forced with different CO_2 concentrations was estimated by comparing the O1-simulated climate with a simulation at 1979 atmospheric CO_2. Mean global surface temperature (air over the land and sea surface for the oceans) was predicted to be 0.26°C cooler in the O1 simulation, but with no noticeable change in the distribution and magnitude of the model bias versus contemporary observations.

Surface temperature and precipitation for non-Antarctic land areas were taken from the terrestrial climatology of New et al. (1999; available online at http://ipcc-ddc.cru.uea.ac.uk/obs/cru_climatologies.html). The mean monthly 1961–90 0.5° dataset was used, converted to seasonal values, and aggregated to the GCM resolution of 4° latitude × 5° longitude (2° latitude at the poles).

For the oceans, the mean monthly observational SSTs used to specify the ocean heat transport were used. These were the 1876–85 period of the Met Office Hadley Centre's sea ice and SST dataset (HadISST1; Rayner et al. 2003). These 1° data were converted to seasonal means and then aggregated to the GCM resolution.

Observational mean seasonal precipitation over the oceans was derived from the Global Precipitation Climatology Project (GPCP) Version 2 Combined Precipitation 2.5° Data Set (Huffman and Bolvin 2005). An earlier version of this dataset was described by Huffman et al. (1997). This dataset starts in 1979, and the 1979–90 period was used. Mean seasonal values were gridded to the GCM resolution and global climate fields produced by merging land values from the CRU dataset with ocean values for temperature from the National Centers for Environmental Prediction (NCEP) and for precipitation from GPCP, with filtering using the GCM land mask.

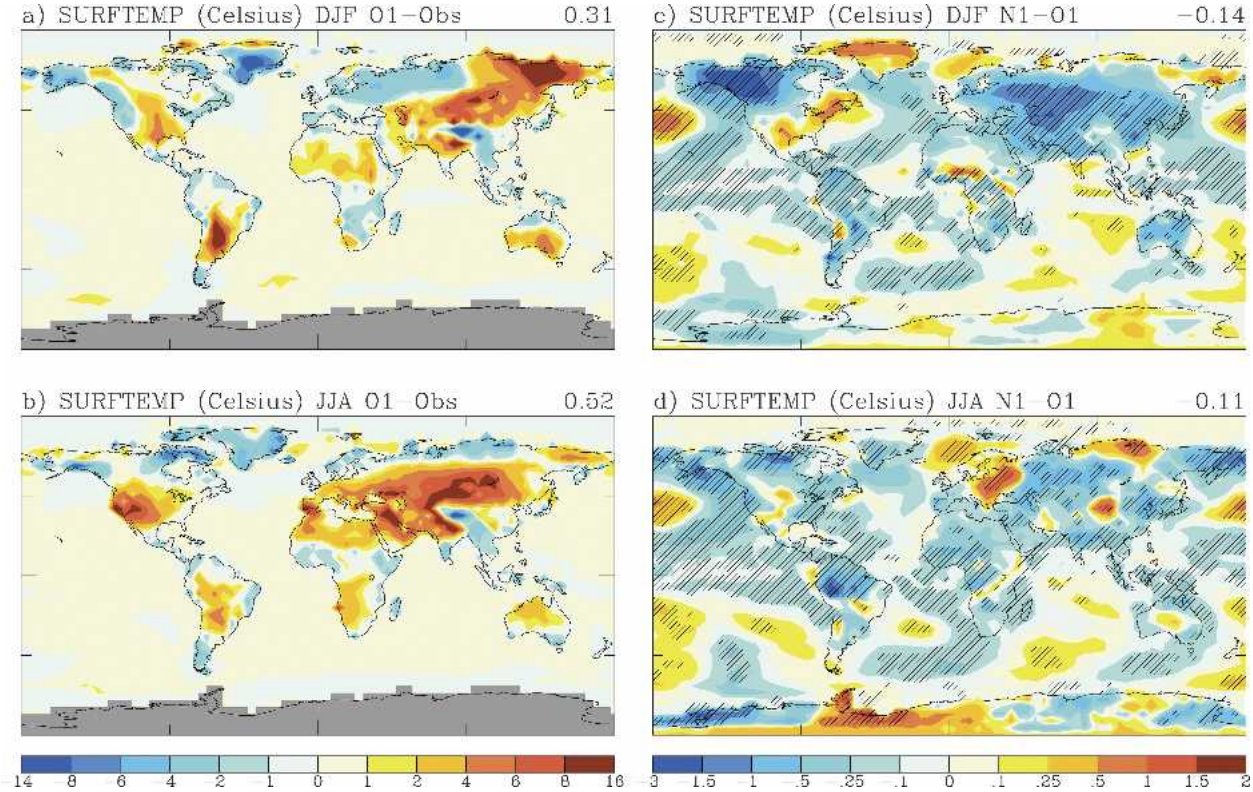

FIG. 3. GISS GCM seasonal mean surface temperature bias using RA97 canopy stomatal conductance submodel in (a) DJF (−13.6° to +16.1°C) and (b) JJA (−12.5° to +12.9°C), and change due to new conductance submodel in (c) DJF (−2.8° to +1.2°C) and (d) JJA (−2.2° to +1.8°C). Observations are surface air temperature over land (New et al. 1999) and SSTs for oceans (Rayner et al. 2003). Global means at upper-right corners. Hatched areas significant at 95% confidence level for a paired *t* test.

Observational cloud cover was extracted from the International Satellite Cloud Climatology Project (ISCCP) stage-D2 (monthly) data product (Rossow and Duenas 2004). Seasonal 2.5° means for 1983–2001 were gridded to the GCM resolution.

4. Global simulations

a. Control climate

1) SURFACE TEMPERATURE

Simulation O1 is compared with observed mean seasonal surface temperatures (i.e., surface air temperature for land, SSTs for ocean) in Figs. 3a,b. A warm model bias occurs over the land in both seasons, but with substantial regional variation. The largest warm biases (>6°C) in December–January–February (DJF) occur over Siberia and central Asia, northern India, and the Paraguay River basin, and in June–July–August (JJA) over large areas of the northern midlatitude landmasses, particularly central Eurasia, the Middle East, the Iberian peninsula, and the western United States. A number of other areas, such as Australia (all year) and southern Africa (in JJA), have lower but significant warm biases of 1°–6°C.

Smaller cool biases are fairly extensive over Europe and southern Africa in DJF, northern Canada and Eurasia in JJA, and Greenland, the Tibetan Plateau, and coastal northwestern North America all year.

Ocean biases are not evident as heat transports were derived from the same SST dataset as the observations.

2) PRECIPITATION

Annual global precipitation simulated in O1 is about 12% higher than observed. Prominent positive biases occur over the tropical oceans and are >4 mm day^{-1} over parts of the western Pacific and Indian Ocean in both seasons and over the equatorial Atlantic in JJA (Figs. 4a,b). In contrast, negative biases of >1 mm day^{-1} occur over many land areas, particularly much of South America and Borneo in DJF, and northern South America and central and western Africa in JJA. The Himalayan region is also too dry in JJA. A less negative but extensive dry bias stretches from the southern

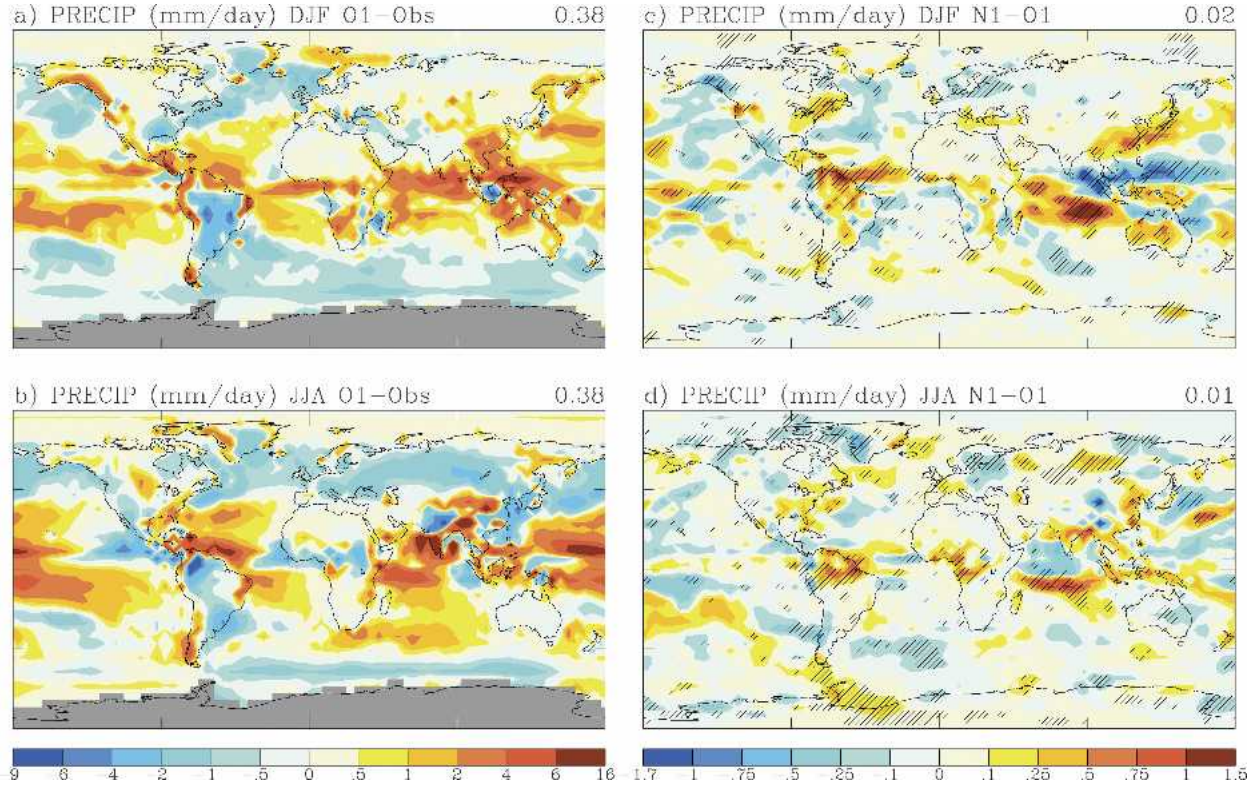

FIG. 4. GISS GCM seasonal mean precipitation bias using RA97 canopy stomatal conductance submodel in (a) DJF (−7.1 to +9.3 mm day^{-1}) and (b) JJA (−8.7 to +15.9 mm day^{-1}), and change due to new conductance submodel in (c) DJF (−1.4 to +1.5 mm day^{-1}) and (d) JJA (−1.7 to +1.1 mm day^{-1}). Observations over land from New et al. (1999) and over oceans from Huffman and Bolvin (2005; see text). Global means at upper-right corners. Hatched areas are significant at 95% confidence level for a paired *t* test.

United States across the North Atlantic in DJF and across much of the northern midlatitudes in JJA.

3) CLOUD COVER

In DJF, northern high latitudes have too much cloud cover by 20%–40% in simulation O1, while the midwestern to southeastern United States and almost all of South America, Africa, southern Eurasia, and Australia have too low cloud cover by 20%–50% (Fig. 5a). In JJA, most land areas are deficient, in places up to 50% (Fig. 5b). The Andes are predicted to have too much cloud cover in both DJF and JJA.

b. Climate response to new canopy stomatal conductance submodel

1) SURFACE TEMPERATURE

Mean global temperature is reduced 0.14°C in DJF and 0.11°C in JJA by the new canopy stomatal conductance submodel (Figs. 3c,d). The largest reductions (>1.5°C) occur over northwestern North America and central Eurasia in DJF. Significant reductions also occur over many tropical landmasses during DJF, particularly northern South America (0.5°–2°C). Many tropical SSTs are also reduced in DJF, but there are also some increases, particularly in the northern Pacific. Significant warming of up to 1°C occurs in DJF over parts of the Sahel, Chile, and northeastern North America and Greenland.

Most land areas are also cooled in JJA, particularly northern South America (0.5°–1.5°C), west and central Africa, central Eurasia, southern Asia, and eastern Siberia. Significant warming of 1°–1.5°C occurs over a large part of eastern Europe, the Tibetan Plateau, and northern Eurasia. SST changes are similar to DJF.

Many of these changes, although not all, are improvements over the O1 simulation.

2) PRECIPITATION

The new canopy stomatal conductance submodel slightly increases mean global precipitation, but there are a number of significant regional changes, particularly in the Tropics (Figs. 4c,d). The largest changes (increases >1 mm day^{-1}) are bipolar between the Indian Ocean and Maritime Continent (decreases >1 mm

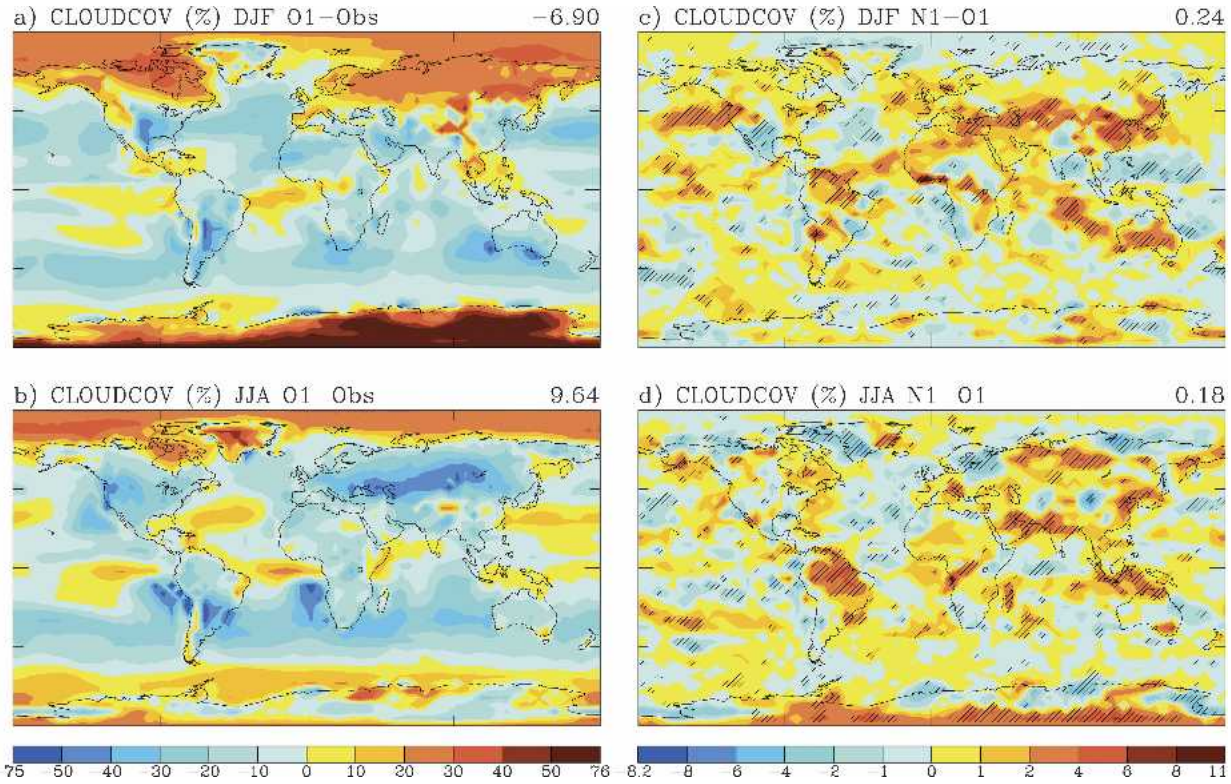

FIG. 5. GISS GCM seasonal mean cloud cover bias using RA97 canopy stomatal conductance submodel in (a) DJF (−55.9% to +75.5%) and (b) JJA (−75.2% to +48.9%), and change due to new conductance submodel in (c) DJF (−4.7% to +11.8%) and (d) JJA (−8.0% to +9.4%). Observations from ISCCP (see text). Global means at upper-right corners. Hatched areas are significant at 95% confidence level for a paired *t* test.

day^{-1}) in DJF. Large increases occur in DJF over parts of South America and the equatorial Atlantic, west Africa, Australia, the western United States, northeastern North America, and southern China.

In JJA, much of northern South America experiences increased precipitation, as do central and west Africa, central Eurasia, and a large part of the Indian Ocean. Eastern Europe dries in both seasons, and the Tibetan Plateau dries in JJA. A strong bipolar response occurs over the Pacific east of Japan in JJA.

Increases in year-round precipitation over South America and west Africa, and in JJA over central Eurasia, reduce previous model bias, as do reductions along the northwest North American coast and Maritime Continent in DJF. These changes generally represent improvements of 10%–20%.

3) CLOUD COVER

Inclusion of the new canopy stomatal conductance submodel increases cloud cover by 1%–6% along the Amazon to southwestern Eurasia DJF ITCZ (Fig. 5c), where it was previously 10%–30% too low (Fig. 5a). DJF cloud cover also increases (by 1%–6%) over eastern Asia, and from the Indian Ocean through Australia, where these areas were previously 10%–30% too low. In JJA, the Amazon region and tropical Africa have increased cloud cover of 2%–6%, where it was previously 10%–30% too low. The previously low cloud amounts over the Iberian Peninsula through to eastern Asia, and from India to southeast Asia, show significant increases in JJA, while significant decreases occur over the Tibetan Plateau and Aral Sea where cover was previously too high.

4) CANOPY STOMATAL CONDUCTANCE

All statistically significant differences between simulations N1 and O1 must result ultimately from changes in modeled canopy stomatal conductance. Figure 6 shows this forcing.

Mean seasonal N1 canopy stomatal conductance is higher than O1 in most regions, with the largest increases in tropical rain forests [typically +5 $mm_{(H2O)}$ s^{-1}, about 50%]. Large increases also occur in DJF across southern Africa and northern Australia, and in

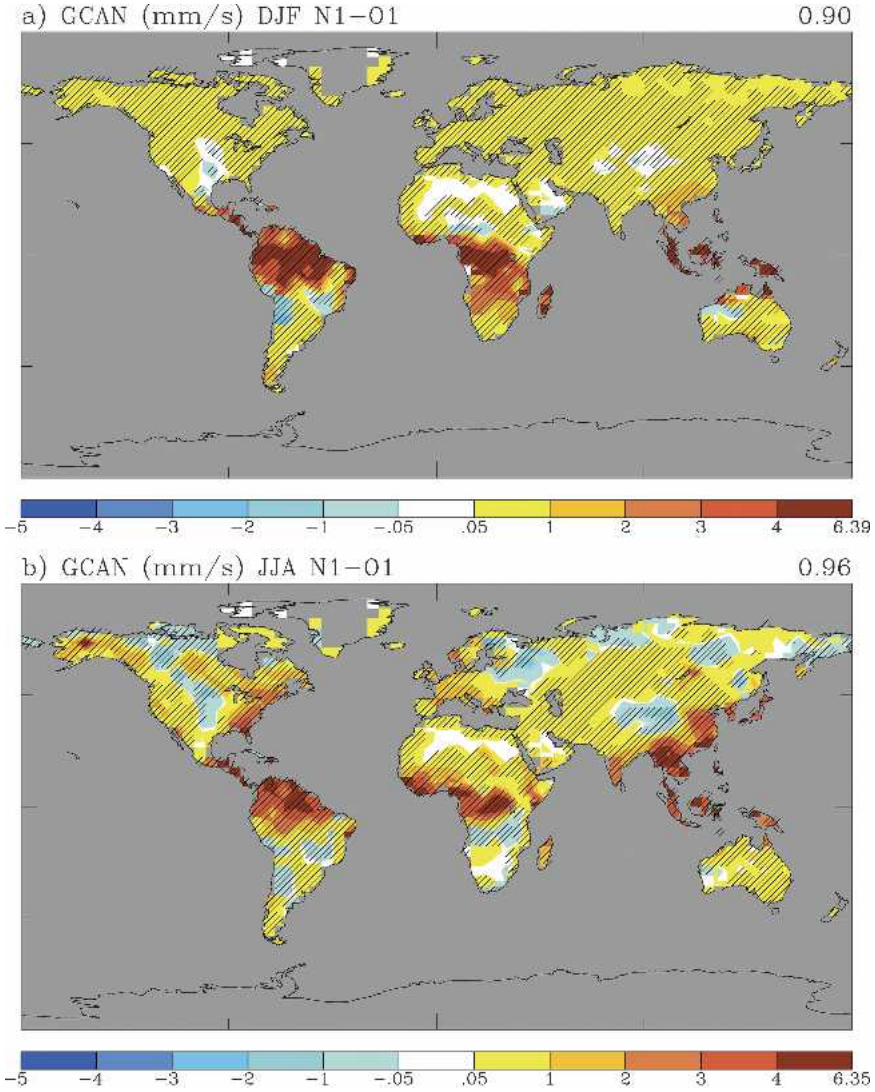

FIG. 6. Change in mean seasonal canopy stomatal conductance to moisture between GISS GCM simulations using RA97 and the new conductance submodel in (a) DJF (−3.0 to +6.4 mm s^{-1}) and (b) JJA (−2.7 to +6.3 mm s^{-1}). Global non-Antarctic land means at upper-right corners. Hatched areas are significant at 95% confidence level for a paired *t* test.

JJA across eastern North America, Alaska, Europe, and southern Asia.

Decreased conductance occurs in a number of regions, including parts of South America, central Sahel, and the central United States in DJF and much of northern Canada and the central United States, and parts of South America, southern Africa, eastern Europe, Tibetan Plateau, and Siberia in JJA.

5. Discussion

There has been considerable debate in the literature concerning the extent to which stomatal conductance controls transpiration at regional scales. In their influential study, Jarvis and McNaughton (1986) argued that negative feedbacks reduce the degree to which stomatal conductance can affect transpiration at increasingly large spatial scales. In particular, they argued that lower transpiration through reduced stomatal conductance would reduce air humidity and increase canopy temperature, leading to an increase in the humidity gradient between the canopy and the atmosphere, and hence to increased transpiration. This negative feedback would dominate at large scales, making stomatal control much less important than the supply of energy.

Subsequent field (e.g., Baldocchi et al. 1997) and

modeling (e.g., Jacobs 1994; Friend and Cox 1995) studies, however, suggest that stomata can have a major impact on regional transpiration. This is largely because of their sensitivity to the leaf-to-air humidity deficit, a strong positive feedback not considered in the analysis of Jarvis and McNaughton (1986). Declining stomatal conductance with humidity deficit reduces transpiration and hence atmospheric moisture, further increasing the humidity deficit. The same rationale for the increased importance of negative feedbacks with spatial scale in the study of Jarvis and McNaughton (1986) also applies to this positive feedback, allowing stomatal control a significant role in large-scale atmospheric processes, especially from tall vegetation (McNaughton and Jarvis 1991; Friend and Cox 1995). The manner in which the stomatal sensitivity to humidity is represented has a major impact on simulated vegetation–atmosphere interactions (cf. Jacobs 1994; Friend and Cox 1995).

The model results presented here strongly support the view that stomata can have a major influence on the atmosphere, even at the largest of scales, although it should be recognized that the climatic effect of stomatal control on transpiration is model dependent. Inclusion of a relatively realistic canopy stomatal conductance model in the GISS GCM has significant effects on simulated climate, many of which reduce previous model bias. It is not possible to analyze fully all processes and feedbacks leading to each of these effects, but some of the most significant are discussed below.

a. Tropical rain forest

The significant reductions in surface air temperature over tropical forests, particularly over South America (Fig. 3), are associated with regions of increased precipitation (Fig. 4) and canopy stomatal conductance (Fig. 5), reducing model bias. Over central Amazonia, for example, some previous model biases of +2°C are reduced by 1°C. Temperatures are lowered as a result of increased latent heat flux (mean evaporation increases by about 0.3 mm day^{-1}) and cloud cover (increases of 2% to 6%: Fig. 5), with mean incident radiation reduced by about 3 W m^{-2}.

These changes result both from higher absolute conductances at high light (Fig. 1) and from humidity–conductance feedbacks at high humidity. Figure 7 demonstrates the importance of the positive feedback with atmospheric humidity not possible with RA97, showing a large increase in specific humidity over the Amazon rain forest in JJA [note that the largest changes occur where mean specific humidity is about 11.5 g kg^{-1} (Figs. 7a,b), where the old and new submodels coincide (Fig. 1f)]. Lower canopy temperatures contribute to the reduction in Δ by lowering q_{can} [(9)], with about 50% of the conductance increase ultimately resulting from the change in Δ (the relative response to humidity is higher in DJF because Δ is lower; Fig. 1f).

These increases in canopy conductance and transpiration cause greater continental recycling of water and moisture convergence over the Amazon. Mean seasonal soil moisture increases between 15% and 20% compared to RA97, while annual river discharge falls by up to 10%. The increase in soil moisture produces a further positive feedback through its effect on stomatal conductance.

These responses, and the comparisons between the old and new conductance submodels and the Amazon rain forest flux data (Fig. 2), suggest that specification of rain forest canopy stomatal conductance is critical for correct simulation of surface energy budgets and regional hydrology. The higher peak tropical rain forest conductance in the new scheme results directly from the addition of a leaf-to-air humidity deficit response, combined with a more realistic response to incident radiation (Figs. 1 and 2). These findings are consistent with recent modeling studies showing the importance of surface conductance for tropical climates (e.g., Hales et al. 2004). Substantial model bias over tropical rain forests remains, however, and is likely due to persistent problems with nonsurface model physics (G. Schmidt 2004, personal communication).

b. West Africa

The climate response to the new canopy stomatal conductance submodel over west Africa is interesting, with significant regional increases and decreases in DJF temperature (Fig. 3c). A large region of the central Sahel, dominated by savanna vegetation, warms by >0.5°C, whereas the coastal tropical rain forest cools by a similar amount. Coastal precipitation, cloud cover, and humidity all increase, whereas farther north and east, air humidity is reduced. Figure 7 shows again the important role of positive conductance feedbacks with atmospheric humidity. Conductance falls across the central Sahel, where original air humidity was low (Fig. 7a). On the other hand, it appears that moisture from more southerly oceanic air masses is drawn to the coastal region. Precipitation and cloud cover were originally too high over the ocean, but this bias is reduced by the new scheme, with greater moisture convergence above the coastal rain forest in response to greater convective heating. Soil moisture is increased both in the coastal zone (by around 30%) and the central Sahel (by 5%–10%). The former increase is due to increased precipitation as evaporation either increases or is unchanged. However, evaporation over the Sahel is reduced as a result of the greater stomatal

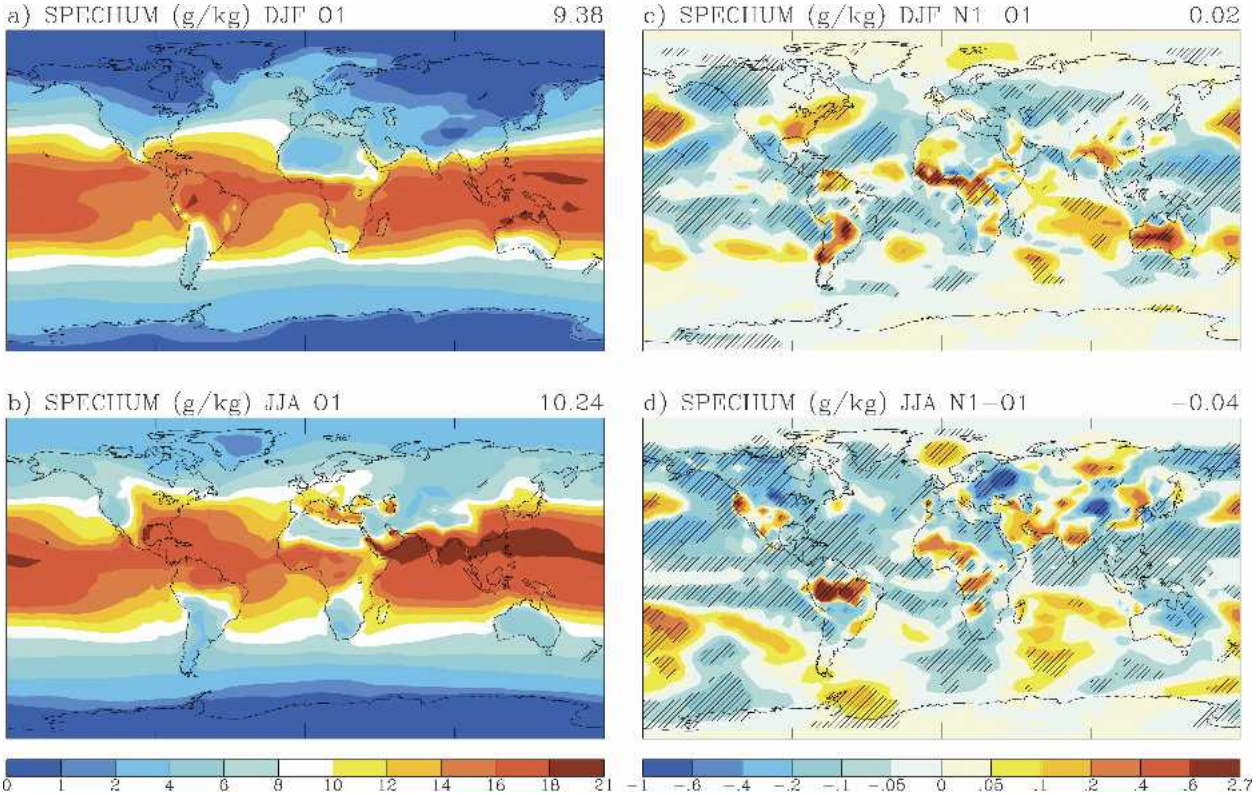

FIG. 7. Mean seasonal surface level atmospheric specific humidity predicted by the GISS GCM using RA97 canopy stomatal conductance submodel in (a) DJF and (b) JJA, and change resulting from using new conductance submodel in (c) DJF (−0.78 to +1.35 g kg^{-1}) and (d) JJA (−1.03 to +2.70 g kg^{-1}). Global means at upper-right corners. Hatched areas are significant at 95% confidence level for a paired *t* test.

closure, thereby conserving soil moisture. Specification of relatively low canopy N and n_f for shrub and woodland vegetation (Table 1) contributes to this effect and to the positive feedback with atmospheric humidity over the Sahel.

c. Central Eurasia and northwestern North America

Significant cooling occurs across central Eurasia and northwestern North America in response to the new canopy stomatal conductance scheme (Fig. 3). Precipitation reductions occur along the Alaskan coast in DJF, and increases occur in central Eurasia in JJA; both changes reduce model bias (Fig. 4). However, local changes in mean canopy stomatal conductance are small (Fig. 6).

The DJF changes are clearly not correlated with local vegetation state. The vegetation is dormant at this time, and evaporation is not affected by the choice of submodel. Incident radiation is not changed either in DJF, although there are some reductions in JJA where cloud cover increases, contributing to regional cooling. Soil moisture is up to about 15% higher in DJF, and the regional distribution of this change is correlated with increased JJA conductance and evaporation.

The DJF climate response in these regions to the new canopy stomatal conductance submodel must therefore be nonlocal. It is well known that changes in tropical latent heating (such as those due to ENSO) impact extratropical atmospheric circulation (Diaz and Kiladis 1992), and this appears to be the case here, but with the forcing originating from the tropical land surface.

The NH 500-hPa height response to the new conductance submodel has a strong pattern in DJF (Fig. 8), with reduced height centered over western Canada, surrounded by a ring of increased height, with a maximum increase of 32.4 m over the northeast Pacific and another zone of reduced height over central Eurasia. This pattern is similar to that observed during La Niña years (Hoerling et al. 1997) and opposite to changes observed as tropical SSTs have increased during the second half of the twentieth century (Hoerling et al. 2001). This suggests that extratropical atmospheric responses to cool tropical oceans (caused by La Niña),

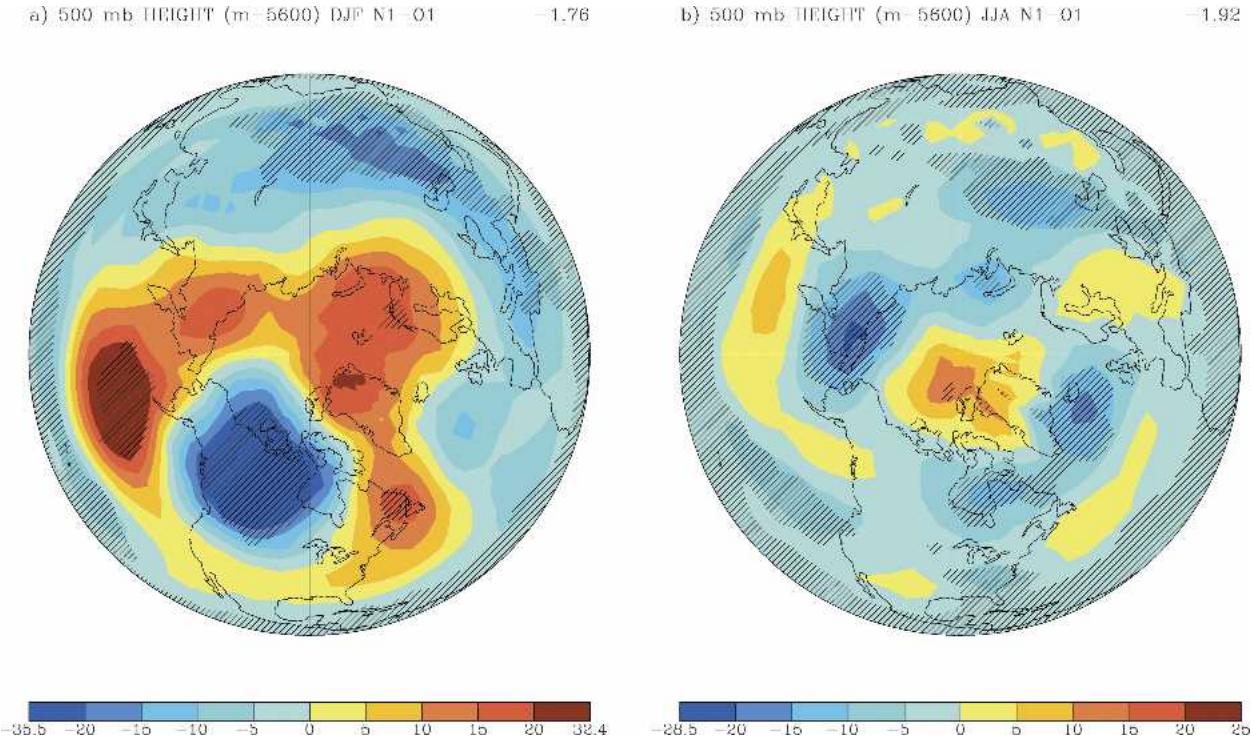

FIG. 8. The NH 500-hPa height change between GISS GCM simulation using canopy stomatal conductance submodel RA97 and new conductance submodel in (a) DJF (−35.5 to +32.4 m) and (b) JJA (−28.5 to +17.7 m). Global means at upper-right corners. Hatched areas are significant at 95% confidence level for a paired *t* test.

and the N1 response to reduced tropical land surface temperatures (caused by increased canopy conductance), may have similar mechanisms. Trenberth and Branstator (1992) showed how, during La Niña years, the location and intensity of the ITCZ changes as a result of changed SSTs. This is also found here, but initiated by changes in convective heating over land, with significant shifts in tropical precipitation patterns over land and ocean (Figs. 4c,d), generally resulting in reduced biases in both seasons compared to the original model (Figs. 4a,b).

d. CO_2 fluxes

Mean global canopy net CO_2 flux is 121 $Pg_{(C)}\ yr^{-1}$ in simulation N1, in line with other estimates of global canopy carbon fluxes (Prentice et al. 2001). Photosynthesis and transpiration are closely linked, and therefore this CO_2 flux is evidence of realistic global land surface–atmosphere coupling.

6. Conclusions

The new canopy stomatal conductance model described in this paper is now incorporated into the frozen ModelE1 version of the GISS GCM (SCH). The new submodel includes responses to atmospheric humidity and CO_2 concentration, responses missing from the previous parameterization, as well as more mechanistic representations of the responses to light, temperature, and photosynthetic N, and an effect of canopy height. Scaling to the canopy and different vegetation types uses a small set of parameters, two of which are calibrated using flux data.

The new submodel results in increased mean canopy conductance over much of the land surface, causing surface cooling in many regions previously too warm, and increased atmospheric humidity and moisture convergence where rainfall was previously too low. Remote effects of increased tropical convective heating cause large changes in boreal climate. Positive feedbacks between conductance and atmospheric humidity and responses to light play important roles in these changes.

Realistic representation of the stomatal control on land evaporation is critical for accurate simulation of atmospheric dynamics. Moreover, greater realism in canopy conductance behavior increases the value of the GISS GCM as a tool for assessing impacts of greenhouse gases on climate.

Acknowledgments. We thank Gavin Schmidt and the GISS GCM model development team for producing a versatile code, and especially Reto Ruedy for patient assistance with simulations, Gary Russell and Jean Lerner for software utilities, and Igor Aleinov for technical assistance. Yadvinder Malhi, Paul Berbigier, Denis Loustau, and George Burba provided flux data, and Joe Berry provided leaf N data for Ponca. We thank William B. Rossow and coworkers for production of the ISCCP cloud product. The GPCP combined precipitation data were developed and computed by the NASA Goddard Space Flight Center's Laboratory for Atmospheres as a contribution to the GEWEX Global Precipitation Climatology Project. Jean-Louis Dufresne assisted with interpretation of output, and David Rind and Jacek Chowdhary provided insightful comments. We are indebted to Maxwell Kelley for critical comments on a previous draft of this paper. Partial funding was provided by the Department of Energy, Office of Science (BER) as part of the Scientific Discovery through Advanced Computing (SciDAC) program (grant DE-FG02-02ER63444). We also thank Jack Kaye, Don Anderson, and Tsengdar Lee of NASA Headquarters for support of our research. ADF was partly supported by the CNRS (France).

REFERENCES

Aber, J. D., A. Magill, R. Boone, J. M. Melillo, and P. A. Steudler, 1993: Plant and soil responses to three years of chronic nitrogen additions at the Harvard Forest, Massachusetts. *Ecol. Appl.,* **3,** 156–166.

Abramopoulos, F., C. Rosenzweig, and B. Choudhury, 1988: Improved ground hydrology calculations for global climate models (GCMs): Soil water movement and evapotranspiration. *J. Climate,* **1,** 921–941.

Amthor, J. S., M. L. Goulden, J. W. Munger, and S. C. Wofsy, 1994: Testing a mechanistic model of forest-canopy mass and energy exchange using eddy correlation: Carbon dioxide and ozone uptake by a mixed oak–maple stand. *Aust. J. Plant Physiol.,* **21,** 623–651.

Baldocchi, D., C. A. Vogel, and B. Hall, 1997: Seasonal variation of energy and water vapor exchange rates above and below a boreal jack pine forest canopy. *J. Geophys. Res.,* **102** (D24), 28 939–28 952.

——, and Coauthors, 2001: FLUXNET: A new tool to study the temporal and spatial variability of ecosystem-scale carbon dioxide, water vapor, and energy flux densities. *Bull. Amer. Meteor. Soc.,* **82,** 2415–2434.

Ball, J. T., I. E. Woodrow, and J. A. Berry, 1987: A model predicting stomatal conductance and its contribution to the control of photosynthesis under different environmental conditions. *Progress in Photosynthesis Research,* Vol. 4, J. Biggins, Ed., Martinus Nijhoff Publishers, 221–224.

Berbigier, P., J.-M. Bonnefond, and P. Mellmann, 2001: CO_2 and water vapour fluxes for 2 years above Euroflux forest site. *Agric. For. Meteor.,* **108,** 183–197.

Bernacchi, C. J., E. L. Singsaas, C. Pimental, A. R. Portis Jr., and S. P. Long, 2001: Improved temperature response functions for models of Rubisco-limited photosynthesis. *Plant Cell Environ.,* **24,** 253–259.

Bonan, G. B., 1995: Land–atmosphere CO_2 exchange simulated by a land surface process model coupled to an atmospheric general circulation model. *J. Geophys. Res.,* **100** (D2), 2817–2831.

Buckley, T. N., K. A. Mott, and G. D. Farquhar, 2003: A hydromechanical and biochemical model of stomatal conductance. *Plant Cell Environ.,* **26,** 1767–1785.

Carswell, F. E., and Coauthors, 2000: Photosynthetic capacity in a central Amazonian rain forest. *Tree Physiol.,* **20,** 179–186.

Choudhury, B. J., R. J. Reginato, and S. B. Idso, 1986: An analysis of infrared temperature observations over wheat and calculation of latent heat flux. *Agric. For. Meteor.,* **37,** 75–88.

Clark, D. A., 2004: Sources or sinks? The responses of tropical forests to current and future climate and atmospheric composition. *Philos. Trans. Roy. Soc. London,* **359B,** 477–491.

Cowan, I. R., and G. D. Farquhar, 1977: Stomatal function in relation to leaf metabolism and environment. *Proc. Society for Experimental Biology Symp.: Integration of Activity in the Higher Plant,* Vol. 31, Durham, United Kingdom, Society for Experimental Biology, 471–505.

Cox, P. M., R. A. Betts, C. B. Bunton, R. L. H. Essery, P. R. Rowntree, and J. Smith, 1999: The impact of new land surface physics on the GCM simulation of climate and climate sensitivity. *Climate Dyn.,* **15,** 183–203.

Davidson, E. A., E. Belk, and R. D. Boone, 1998: Soil water content and temperature as independent or confounded factors controlling soil respiration in a temperate mixed hardwood forest. *Global Change Biol.,* **4,** 217–227.

Deardoff, J. W., 1967: Empirical evidence of the eddy coefficient for heat upon stability above the lowest 50 m. *J. Appl. Meteor.,* **6,** 631–643.

Diaz, H. F., and G. N. Kiladis, 1992: Atmospheric teleconnections associated with the extreme phases of the Southern Oscillation. *El Niño: Historical and Paleoclimatic Aspects of the Southern Oscillation,* H. F. Diaz and V. Markgraf, Eds., Cambridge University Press, 7–28.

Dickinson, R. E., and Coauthors, 2002: Nitrogen controls on climate model evapotranspiration. *J. Climate,* **15,** 278–295.

Farquhar, G. D., S. von Caemmerer, and J. A. Berry, 1980: A biochemical model of photosynthetic CO_2 assimilation in leaves of C_3 species. *Planta,* **149,** 78–90.

Foley, J. A., I. C. Prentice, N. Ramankutty, S. Levis, D. Pollard, S. Sitch, and A. Haxeltine, 1996: An integrated biosphere model of land surface processes, terrestrial carbon balance, and vegetation dynamics. *Global Biogeochem. Cycles,* **10,** 603–628.

Forstreuter, M., 1998: What can we learn from microcosms? *European Forests and Global Change: The Likely Impact of Rising CO_2 and Temperature,* P. G. Jarvis, Ed., Cambridge University Press, 274–292.

Friend, A. D., 1993: The prediction and physiological significance of tree height. *Vegetation Dynamics and Global Change,* A. M. Solomon and H. H. Shugart, Eds., Chapman and Hall, 101–115.

——, 1995: PGEN: An integrated model of leaf photosynthesis, transpiration, and conductance. *Ecol. Modell.,* **77,** 233–255.

——, 2001: Modelling canopy CO_2 fluxes: Are 'big-leaf' simplifications justified? *Global Ecol. Biogeogr.,* **10,** 603–619.

——, and P. M. Cox, 1995: Modelling the effects of atmospheric CO_2 on vegetation–atmospheric interactions. *Agric. For. Meteor.,* **73,** 285–295.

——, H. H. Shugart, and S. W. Running, 1993: A physiology-based gap model of forest dynamics. *Ecology,* **74,** 792–797.

——, A. K. Stevens, R. G. Knox, and M. G. R. Cannell, 1997: A process-based, terrestrial biosphere model of ecosystem dynamics (Hybrid v3.0). *Ecol. Modell.,* **95,** 249–287.

Goulden, M. L., J. W. Munger, S.-M. Fan, B. C. Daube, and S. C. Wofsy, 1996: Measurements of carbon sequestration by long-term eddy covariance: Methods and a critical evaluation of accuracy. *Global Change Biol.,* **2,** 169–182.

Hales, K., J. D. Neelin, and N. Zeng, 2004: Sensitivity of tropical land climate to leaf area index: Role of surface conductance versus albedo. *J. Climate,* **17,** 1459–1473.

Hanan, N. P., G. Burba, S. B. Verma, J. A. Berry, A. Suyker, and E. A. Walter-Shea, 2002: Inversion of net ecosystem CO_2 flux measurements for estimation of canopy PAR absorption. *Global Change Biol.,* **8,** 565–574.

Hansen, J., G. Russell, D. Rind, P. Stone, A. Lacis, S. Lebedeff, R. Ruedy, and L. Travis, 1983: Efficient three-dimensional global models for climate studies: Models I and II. *Mon. Wea. Rev.,* **111,** 609–662.

——, and Coauthors, 2002: Climate forcings in Goddard Institute for Space Studies SI2000 simulations. *J. Geophys. Res.,* **107,** 4347, doi:10.1029/2001JD001143.

Hetherington, A. M., and F. I. Woodward, 2003: The role of stomata in sensing and driving environmental change. *Nature,* **424,** 901–908.

Hoerling, M. P., A. Kumar, and M. Zhong, 1997: El Niño, La Niña, and the nonlinearity of their teleconnections. *J. Climate,* **10,** 1769–1786.

——, J. W. Hurrell, and T. Xu, 2001: Tropical origins for recent North Atlantic climate change. *Science,* **292,** 90–92.

Hollinger, D. Y., F. M. Kelliher, E.-D. Schulze, and B. M. M. Köstner, 1994: Coupling of tree transpiration to atmospheric turbulence. *Nature,* **371,** 60–62.

Huffman, G. J., and D. T. Bolvin, cited 2005: GPCP Version 2 Combined Precipitation Data Set documentation. [Available online at http://www1.ncdc.noaa.gov/pub/data/gpcp/v2/documentation/V2_doc.]

——, and Coauthors, 1997: The Global Precipitation Climatology Project (GPCP) Combined Precipitation Dataset. *Bull. Amer. Meteor. Soc.,* **78,** 5–20.

Jacobs, C. M. J., 1994: Direct impact of atmospheric CO_2 enrichment on regional transpiration. Ph.D. thesis, Wageningen Agricultural University, 179 pp.

——, B. M. M. van den Hurk, and H. A. R. de Bruin, 1996: Stomatal behaviour and photosynthetic rate of unstressed grapevines in semi-arid conditions. *Agric. For. Meteor.,* **80,** 111–134.

Jarvis, A. J., and W. J. Davies, 1998: The coupled response of stomatal conductance to photosynthesis and transpiration. *J. Exp. Bot.,* **49,** 399–406.

Jarvis, P. G., 1976: The interpretation of the variations in leaf water potential and stomatal conductance found in canopies in the field. *Philos. Trans. Roy. Soc. London,* **273B,** 593–610.

——, and K. G. McNaughton, 1986: Stomatal control of transpiration: Scaling up from leaf to region. *Adv. Ecol. Res.,* **15,** 1–49.

Jones, H. G., 1992: *Plants and Microclimate: A Quantitative Approach to Environmental Plant Physiology*. 2d ed. Cambridge University Press, 452 pp.

Koch, G. W., S. C. Sillett, G. M. Jennings, and S. D. Davis, 2004: The limits to tree height. *Nature,* **428,** 851–854.

Kull, O., and B. Kruijt, 1998: Leaf photosynthetic light response: A mechanistic model for scaling photosynthesis to leaves and canopies. *Funct. Ecol.,* **12,** 767–777.

Loustau, D., and H. Cochard, 1991: Utilisation d'une chambre de transpiration portable pour l'estimation de l'evapotranspiration d'un sous-bois de pin maritime à molinie (*Molinia coerulea* L. Moench). *Ann. Sci. For.,* **48,** 29–45.

Malhi, Y., A. D. Nobre, J. Grace, B. Kruijt, M. G. P. Pereira, A. Culf, and S. Scott, 1998: Carbon dioxide transfer over a Central Amazonian rain forest. *J. Geophys. Res.,* **103** (D24), 31 593–31 612.

Matthews, E., 1983: Global vegetation and land use: New high-resolution data bases for climate studies. *J. Climate Appl. Meteor.,* **22,** 474–487.

——, 1984: Prescription of land-surface boundary conditions in GISS GCM II: A simple method based on high-resolution vegetation data bases. NASA Tech. Memo. 86096, National Aeronautics and Space Administration, Greenbelt, MD, 20 pp.

McNaughton, K. G., and P. G. Jarvis, 1991: Effects of spatial scale on stomatal control of transpiration. *Agric. For. Meteor.,* **54,** 279–302.

Meir, P., J. Grace, J. Lloyd, and A. C. Miranda, 1996: Soil respiration in a rain forest in Amazonia, and in cerrado in Central Brazil. *Amazonian Climate and Deforestation,* J. H. C. Gash et al., Eds., J. M. Wiley and Sons, 319–330.

Mencuccini, M., S. Mambelli, and J. Comstock, 2000: Stomatal responsiveness to leaf water status in common bean (*Phaseolus vulgaris* L.) is a function of time of day. *Plant Cell Environ.,* **23,** 1109–1118.

Monteith, J. L., 1973: *Principles of Environmental Physics*. Edward Arnold, 241 pp.

Morison, J. I. L., 1998: Stomatal response to increased CO_2 concentration. *J. Exp. Bot.,* **49,** 443–452.

Mott, K. A., and D. F. Parkhurst, 1991: Stomatal responses to humidity in air and helox. *Plant Cell Environ.,* **14,** 509–515.

New, M., M. Hulme, and P. Jones, 1999: Representing twentieth-century space–time climate variability. Part I: Development of a 1961–90 mean monthly terrestrial climatology. *J. Climate,* **12,** 829–856.

Nobel, P. S., 1991: *Physicochemical and Environmental Plant Physiology.* 2d ed. Academic Press, 474 pp.

Oke, T. R., 1987: *Boundary Layer Climates.* 2d ed. Routledge, 450 pp.

Porté, A., and D. Loustau, 1998: Variability of the photosynthetic characteristics of mature needles within the crown of a 25-year-old *Pinus pinaster. Tree Physiol.,* **18,** 223–232.

Prentice, I. C., and Coauthors, 2001: The carbon cycle and atmospheric carbon dioxide. *Climate Change 2001: The Scientific Basis,* J. T. Houghton et al., Eds., Cambridge University Press, 183–237.

Press, W. H., B. P. Flannery, S. A. Teukolsky, and W. T. Vetterling, 1989: *Numerical Recipes. "Fortran version."* Cambridge University Press, 702 pp.

Rayner, N. A., D. E. Parker, E. B. Horton, C. K. Folland, L. V. Alexander, D. P. Rowell, E. C. Kent, and A. Kaplan, 2003: Global analyses of sea surface temperature, sea ice and night marine air temperature since the late nineteenth century. *J. Geophys. Res.,* **108,** 4407, doi:10.1029/2002JD002670.

Rosenzweig, C., and F. Abramopoulos, 1997: Land-surface model development for the GISS GCM. *J. Climate,* **10,** 2040–2054.

Rossow, W. B., and E. N. Duenas, 2004: The International Satellite Cloud Climatology Project (ISCCP) Web site—An online resource for research. *Bull. Amer. Meteor. Soc.,* **85,** 167–172.

Sellers, P. J., and Coauthors, 1996: A revised land surface parameterization (SiB2) for atmospheric GCMs. Part I: Model formulation. *J. Climate,* **9,** 676–705.

Spitters, C. J. T., 1986: Separating the diffuse and direct component of global radiation and its implications for modeling canopy photosynthesis. Part II. Calculation of canopy photosynthesis. *Agric. For. Meteor.,* **38,** 231–242.

——, H. A. J. M. Toussaint, and J. Goudriaan, 1986: Separating the diffuse and direct component of global radiation and its implications for modeling canopy photosynthesis. Part I. Components of incoming radiation. *Agric. For. Meteor.,* **38,** 217–229.

Trenberth, K. E., and G. W. Branstator, 1992: Issues in establishing causes of the 1988 drought over North America. *J. Climate,* **5,** 159–172.

von Caemmerer, S., and G. D. Farquhar, 1981: Some relationships between the biochemistry of photosynthesis and the gas exchange of leaves. *Planta,* **153,** 376–387.

White, M. A., P. E. Thornton, S. W. Running, and R. R. Nemani, 2000: Parameterization and sensitivity analysis of the BIOME-BGC terrestrial ecosystem model: Net primary production controls. *Earth Interactions,* **4.** [Available online at http://EarthInteractions.org.]

Williams, M., Y. Malhi, A. D. Nobre, E. B. Rastetter, J. Grace, and M. G. P. Pereira, 1998: Seasonal variation in net carbon exchange and evapotranspiration in a Brazilian rain forest: A modelling analysis. *Plant Cell Environ.,* **21,** 953–968.

Wofsy, S. C., M. L. Goulden, J. W. Munger, S. M. Fan, P. S. Bakwin, B. C. Daube, S. L. Bassow, and F. A. Bazzaz, 1993: Net exchange of CO_2 in a midlatitude forest. *Science,* **260,** 1314–1317.

Wong, S. C., I. R. Cowan, and G. D. Farquhar, 1979: Stomatal conductance correlates with photosynthetic capacity. *Nature,* **282,** 424–426.

Zeiger, E., G. D. Farquhar, and I. R. Cowan, Eds., 1987: *Stomatal Function.* Stanford University Press, 519 pp.